11

Photonic crystal structures with tunable resonance

© A.A. Syrov, S.V. Tomilin, A.L. Kudryashov, S.D. Lyashko, O.A. Tomilina

V.I. Vernadsky Crimean Federal University, Simferopol, Russia

e-mail: anatoly199824@rambler.ru

Received June 19, 2025
Revised August 20, 2025
Accepted October 30, 2025

The paper presents experimental results of synthesis and characterization of photonic crystalline structures based on Bragg mirrors containing optical half-wavelength vanadium dioxide defect layers with the possibility of parametric and thermal tuning of resonance conditions. The influence of the thickness and optical characteristics of the vanadium dioxide functional layer on the excitation features of optical Fabry-Perot resonance modes is demonstrated. A temperature hysteresis of the optical and resonant characteristics of photonic crystal structures containing a VO_2 layer has been discovered in the vicinity of the phase transition point from semiconductor to metal.

Keywords: photonic crystal, Fabry-Perot resonance, vanadium dioxide, phase transition, spectral shift, temperature hysteresis.

DOI: 10.61011/EOS.2026.01.63225.8283-25

1. Introduction

In recent decades, the study of photonic crystal structures has been one of the advanced spheres of optics and photonics, opening up new horizons in design of the highly efficient optical devices [1–6]. These structures are capable of controlling the propagation of light waves with high accuracy and efficiency, which is used in integrated optical systems, lasers, and data transmission devices. Of particular importance are photonic crystal structures with tunable resonance, which allow fine-tuning the resonant frequencies and resonance width, as well as dynamically changing the optical properties of the system exposed to external environment (temperature, pressure), to create adaptive optical devices, sensors, quantum information elements and optical data processing systems [7–13]. Vanadium dioxide (VO_2) is one of the promising materials, demonstrating a rapid and reversible change in its physical characteristics during a first-order phase transition „semiconductor–metal" [14]. The phase transition is accompanied by a change in the symmetry of the crystal lattice and has a significant effect on the electrical and optical properties of the material. In the semiconductor phase VO_2 has a monoclinic symmetry, and in the metallic phase it acquires tetragonal symmetry; this change in symmetry leads to a drastic change in the electronic structure, which, in turn, affects the conductivity of the material. In particular, VO_2 demonstrates a dramatic change in electrical conductivity and optical properties at a temperature of about 68 °C, which makes it an ideal candidate for creating tunable photonic elements [15,16]. In particular, in the study [16], it was theoretically shown that in photonic crystals with an optical defect from VO_2, thermal switching of characteristics of the entire resonant structure is possible due to variation of properties of the thermo-optical active layer VO_2 resulting from the 1st kind phase transition „semiconductor–metal". Thus, the use of vanadium dioxide in resonant photonic structures will not only raise their efficiency, but also make it possible to create flexible and compact design for modern optical systems. Thus, the integration of vanadium dioxide into photonic crystal structures with tunable resonance improves their functionality and performance, giving a prospect for further optoelectronics development [17–24].

Accordingly, this study outlines the experimental synthesis and investigation of the properties of functional layers of vanadium dioxide (VO_2) and associated photonic crystals and, in particular, the features of dynamic tuning of their resonant properties through thermal control, making it possible to control the light modes in real time and create new functionality for modern optical systems.

2. Experimental methods

In this study, two photonic crystal resonant structures with different spectral ranges were investigated, consisting of two 4-pair Bragg mirrors, between which there was an optical half-wave defect of VO_2 ($h_{VO_2} \cdot n_{VO_2} = \lambda/2$). The first structure is designed for the visible wavelength range for both the photonic band gap (PBG) and the optical Fabry-Perot resonance. The second structure is similar to the first, but is designed for the near infrared (IR) wavelength range. The functional optical layers of photonic crystals with tunable resonance were synthesized using a vacuum coating system by method of magnetron sputtering „small-size vacuum system TM Magna 09" (R&S Department TM, Zelenograd) [25]. The targets made of initial materials VO_2, SiO_2 and TiO_2 (diameter 76 mm, purity 99.95%) were sputtered using the RF-magnetrons with a frequency of 13.6 MHz and power of 150 W in the argon plasma Ar^+ at $6.6 \cdot 10^{-1}$ Pa. The multilayer structures like photonic crystals (PC) were synthesized by sputtering four pairs of

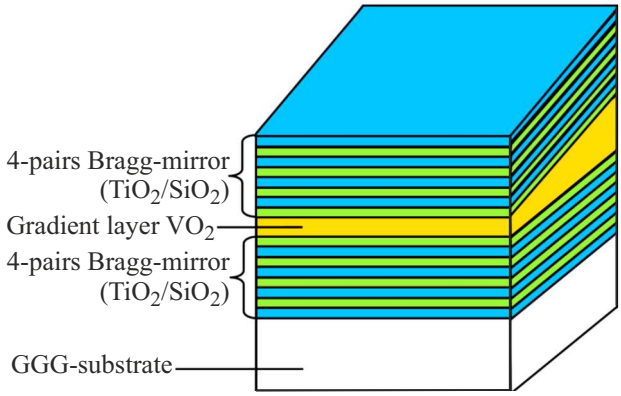

Figure 1. Multi-layered photon-crystalline structure GGG/$[SiO_2/TiO_2]^4/VO_2/[TiO_2/SiO_2]^4$ with a gradient functional layer VO_2.

SiO_2 layers and TiO_2 onto a polished substrate of single-crystal gadolinium gallium garnet $Gd_3Ga_5O_{12}$ (GGG), thus, forming lower Bragg mirror. The thicknesses of the structural layers for SiO_2 and TiO_2 were 110 nm and 71 nm for a photonic crystal in the visible range and 143 nm and 83 nm for a photonic crystal in the IR range, respectively, which corresponds to the optical layer thickness of one quarter of the wavelength ($h_{SiO_2,TiO_2} \cdot n_{SiO_2,TiO_2} = \lambda/4$). After the lower Bragg mirror had been formed a layer of VO_2 with a thickness of half the light wavelength was sputtered onto its surface, which was not consistent with the quarter-wave periodicity of the photonic crystal. To synthesize the functional layer VO_2, the technique to forming a coating with a thickness gradient along the selected direction was used which made it possible to obtain different areas thicknesses in different portions of the sample. The thickness gradient was formed as a result of the material deposition in an inhomogeneous flow formed when flowing around mechanical obstacles [26]. For a 10 mm long sample the thickness VO_2 varied from 120 to 130 nm for the photon crystal in the visible range and from 160 to 170 nm for the photon crystal in IR-range which is consistent with the thickness grad $h = 1$ nm/mm. To achieve optimal homogeneous crystals VO_2 and improve the electrophysical and optical characteristics, as well as to relieve the internal stresses of the film [27], the sample was thermally annealed after the deposition process. The annealing was carried out in the oxygen environment ($P = 6 \cdot 10^{-3}$ Pa) during 120 min at a temperature of 550 °C. Further, upper Bragg mirror consisting of 4 pairs of TiO_2/SiO_2 layers was deposited over the vanadium dioxide functional layer. The final multilayer structure may be described by the structural formula GGG/$[SiO_2/TiO_2]^4/VO_2/[TiO_2/SiO_2]^4$ and schematically described in Fig. 1.

The optical resonance properties of the photon-crystalline structures based on VO_2 layers were investigated using spectrophotometer Holmarc HO-A216FR/KR-ORMSC2 with Czerny–Turner optical configuration within 400–950 nm and spectral permit 2 nm (monochromator output slit width of 0.2 mm). The transmittance spectrum of a sample was determined as the ratio of the intensity of light of a known wavelength transmitted through the sample to the intensity of light incident on the sample (i.e., detected by a photodetector in the absence of a sample):

$$T(\lambda) = \frac{I_s(\lambda) - I_D(\lambda)}{I_0(\lambda) - I_D(\lambda)}, \quad (1)$$

where $I_S(\lambda)$ — spectral dependence of the intensity of light transmitted through the sample, $I_0(\lambda)$ — spectral dependence of the intensity of light incident on the sample, $I_D(\lambda)$ — dark current of the photodetector, obtained under condition that there's no light from the source.

The temperature dependences of the transmittance of photonic crystals were measured using a modified sample holder containing a resistive heater and a thermoresistive temperature sensor. The heater was controlled by AtXMega32A4U microcontroller, temperature control was carried out via pulse-width modulation of the heater current, PID stabilization method [28] was used to stabilize the temperature. The measurements were performed when the sample was heated from room temperature to a temperature above the semiconductor–metal phase transition point, and then the temperature was lowered back to the room temperature to register the temperature hysteresis of optical transmittance.

3. Results and discussion

3.1. Visible range photon crystal

Visible range photon crystal with a structure GGG/$[SiO_2/TiO_2]^4/VO_2/[TiO_2/SiO_2]^4$ and thicknesses of functional layers mentioned in section 2, is itself a Fabry-Perot resonator with a tunable resonance due to the varied thickness of the optical half-wave defect as VO_2 layer. Figure 2 shows the transmittance spectra of this photonic crystal in the range 450–950 nm at room temperature. It can be seen that allowed optical states are formed inside the photonic band gap, which manifest themselves as local transmittance peaks and are caused by the excitation of Fabry-Perot resonant modes at wavelengths from 634 to 670 nm. The spectral position of the transmittance maxima corresponds to conditions of excitation of microresonator modes and depends on the thickness of vanadium dioxide optical layer, provided that a single antinode of the standing wave is formed in it [25]. In this case, thickness increase of VO_2 leads to a spectral shift of the corresponding resonant peak of the Fabry-Perot mode towards a longer wavelength region(„red“ shift).

Fig. 3 illustrates the transmittance spectra of the visible range photon crystal GGG/$[SiO_2/TiO_2]^4/VO_2/[TiO_2/SiO_2]^4$, registered at different temperatures in the range from 19 to 90 °C at a section with the thickness layer VO_2 about $h_{VO_2} = 123$ nm. When the sample is heated and the

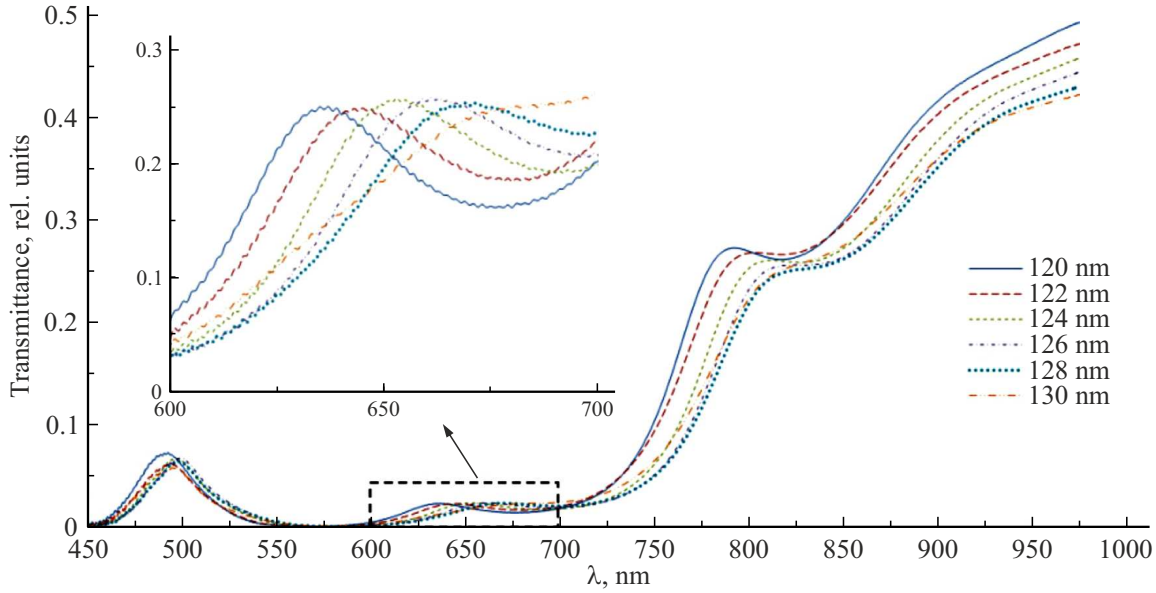

Figure 2. Transmittance spectra of the visible photon-crystalline structure GGG/$[SiO_2/TiO_2]^4/VO_2/[TiO_2/SiO_2]^4$ along the thickness gradient VO_2 (shown in the legend), the inset shows a zoomed in excitation region of the resonant modes.

temperature rises accordingly (Fig. 3, *a*) the resonant peak at $\lambda_{res} = 648$ nm undergoes two types of changes associated with variation of the complex refractive index of VO_2 layer. Thus, a decline in the real part of the refractive index VO_2 with a growing temperature leads to a spectral shift in the position of the transmittance maximum towards shorter wavelengths, while increase in the refractive index imaginary part leads to higher optical absorption in the layer VO_2 and, as a result, to a decrease in amplitude peak transmittance [29,30]. So, when 90 °C is reached a resonant wavelength makes $\lambda_{res} = 614$ nm, and the maximum transmittance is reduced by three times compared to the initial value.

As the sample cools (Fig. 3, *b*), the reverse process of displacement of Fabry-Perot resonance peak and an increase in transmittance at the resonance point is observed. However, it is worth noting that at the same temperatures, the transmittance spectra during heating and cooling of the sample differ, demonstrating a clear temperature hysteresis, despite the fact that the spectra at extreme temperatures (19 and 90 °C) completely match.

The results of investigation of transmittance temperature hysteresis (at different wavelengths) and the resonant wavelength during phase transition in the optical layer VO_2 are shown in Fig. 4. It is clearly seen that variation in the optical constants of VO_2 functional layer results in a fourfold change of the structure transmittance at the wavelength of $\lambda = 647$ nm in the vicinity of Fabry-Perot resonance (Fig. 4, *a*) and a twofold change at $\lambda = 930$ nm beyond the PBG (Fig. 4, *b*). The width of the transmittance temperature hysteresis loop remains unchanged, from about 6 to 8 °C, and is practically independent of the wavelength. In this case, the absolute transmittance values are determined both by the complex dispersion of the optical constants of the layer itself VO_2, associated with electronic transitions [31], and by the optical parameters of the photonic crystal itself, due to the formation of standing waves in the periodic structures of Bragg mirrors.

Fig. 4, *c* illustrates the temperature hysteresis loop for the resonance wavelength of Fabry-Perot mode. It can be seen that the transition temperature and the width of the hysteresis loop are similar to the transmittance temperature hysteresis loops at a fixed wavelength (Fig. 4, *a,b*), while the resonant wavelength λ_{res} itself, as shown above, changes by 34 nm, which corresponds to a change in the optical thickness of the half-wave layer VO_2 by 17 nm.

Thus, it can be seen that in a photonic crystal containing an optical half-wave layer VO_2 with a thickness gradient, it is possible to retune Fabry-Perot optical resonance both parametrically by changing the working area along the thickness gradient of the functional layer VO_2, and thermally by changing its optical constants. While in case of parametric control of resonant properties, the geometric path difference of rays reflected from opposite surfaces of the functional half-wave layer changes, and in case of thermal control, the optical path difference of the same rays changes, leading to a spectral shift in the interference condition thus resulting in formation of nodes and antinodes of the standing wave inside VO_2 layer (Fabry-Perot mode).

3.2. IR range photon crystal

Similar measurements were made for IR-range photon crystal of GGG/ $[SiO_2/TiO_2]^4/VO_2/[TiO_2/SiO_2]^4$, the thickness of functional layers is shown in section 2. Figure 5 shows the transmittance spectra of this photonic crystal

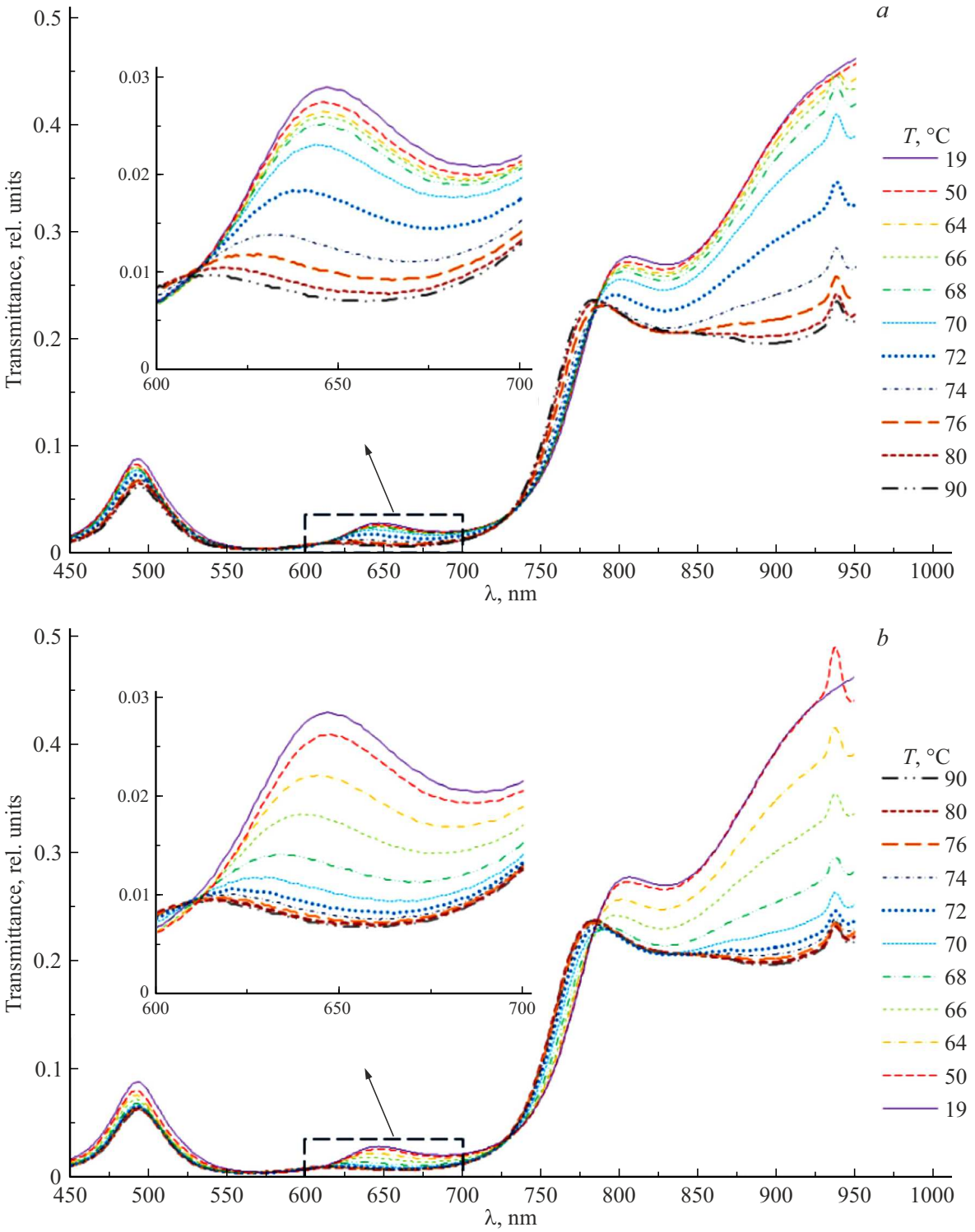

Figure 3. Transmittance spectra of the visible photon-crystalline structure GGG/$[SiO_2/TiO_2]^4/VO_2/[TiO_2/SiO_2]^4$ (thickness $h_{VO_2} = 123$ nm) during temperature variation: (*a*) heating; (*b*) cooling (the insets show enlarged sections).

in the range from 450 to 950 nm at room temperature, obtained in various sections of the thickness gradient of the optical half-wave layer VO_2. Resolved optical states are occurring within PBG in the wavelength range 840–995 nm, which manifest themselves as local transmittance maxima associated with the excitation of Fabry-Perot resonant modes. Here, the increase in thickness of VO_2 layer leads to a change in formation of an optical standing wave and a spectral shift of the resonant peak of the Fabry-Perot mode to a longer wavelength region of the spectrum.

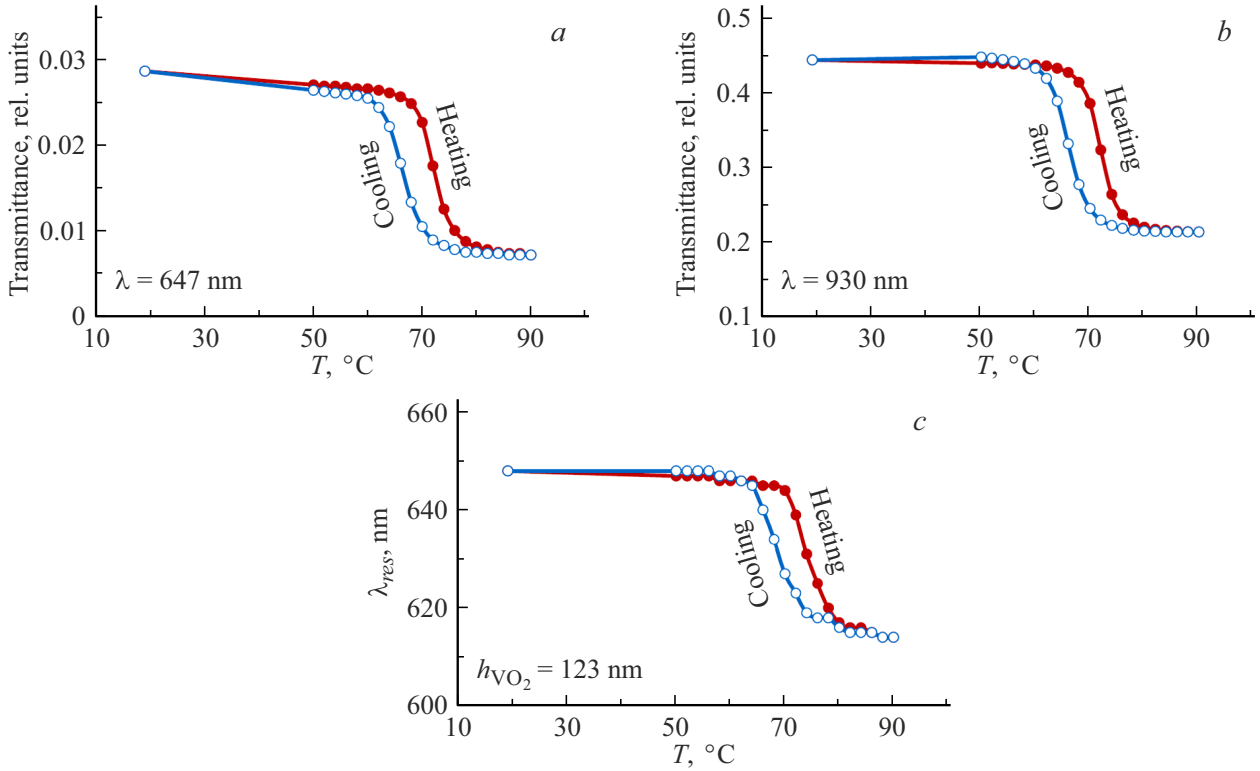

Figure 4. Thermal hysteresis loops of transmittance for the visible range photon-crystalline structure at various wavelengths $\lambda = 647$ nm (a) and $\lambda = 930$ nm (b); thermal hysteresis loop of the resonance wavelength of Fabry-Perot mode (c).

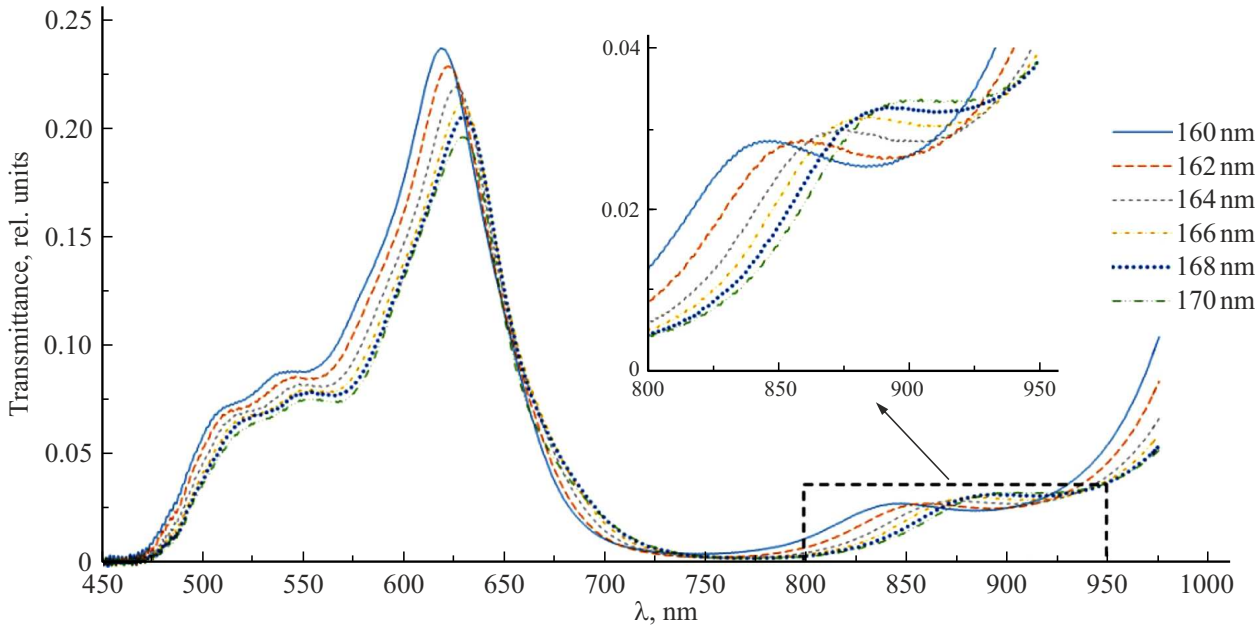

Figure 5. Transmittance spectra of the IR-range photon-crystalline structure GGG/$[SiO_2/TiO_2]^4$/VO_2/$[TiO_2/SiO_2]^4$ along the thickness gradient VO_2 (shown in the legend), the inset shows a zoomed-in excitation region of the resonant modes.

Fig. 6 illustrates the transmittance spectra of IR-range photon crystal GGG/$[SiO_2/TiO_2]^4$/ VO_2/$[TiO_2/SiO_2]^4$, measured at various temperatures varying from 20 to 90 °C, for the gradient thickness of VO_2 layer with $h_{VO_2} = 163$ nm. The change in the optical constants of VO_2 layer is caused by sample heating and a corresponding temperature rise (Fig. 6, a) which affects the excitation conditions of Fabry-Perot resonance located at the wavelength $\lambda_{res} = 862$ nm.

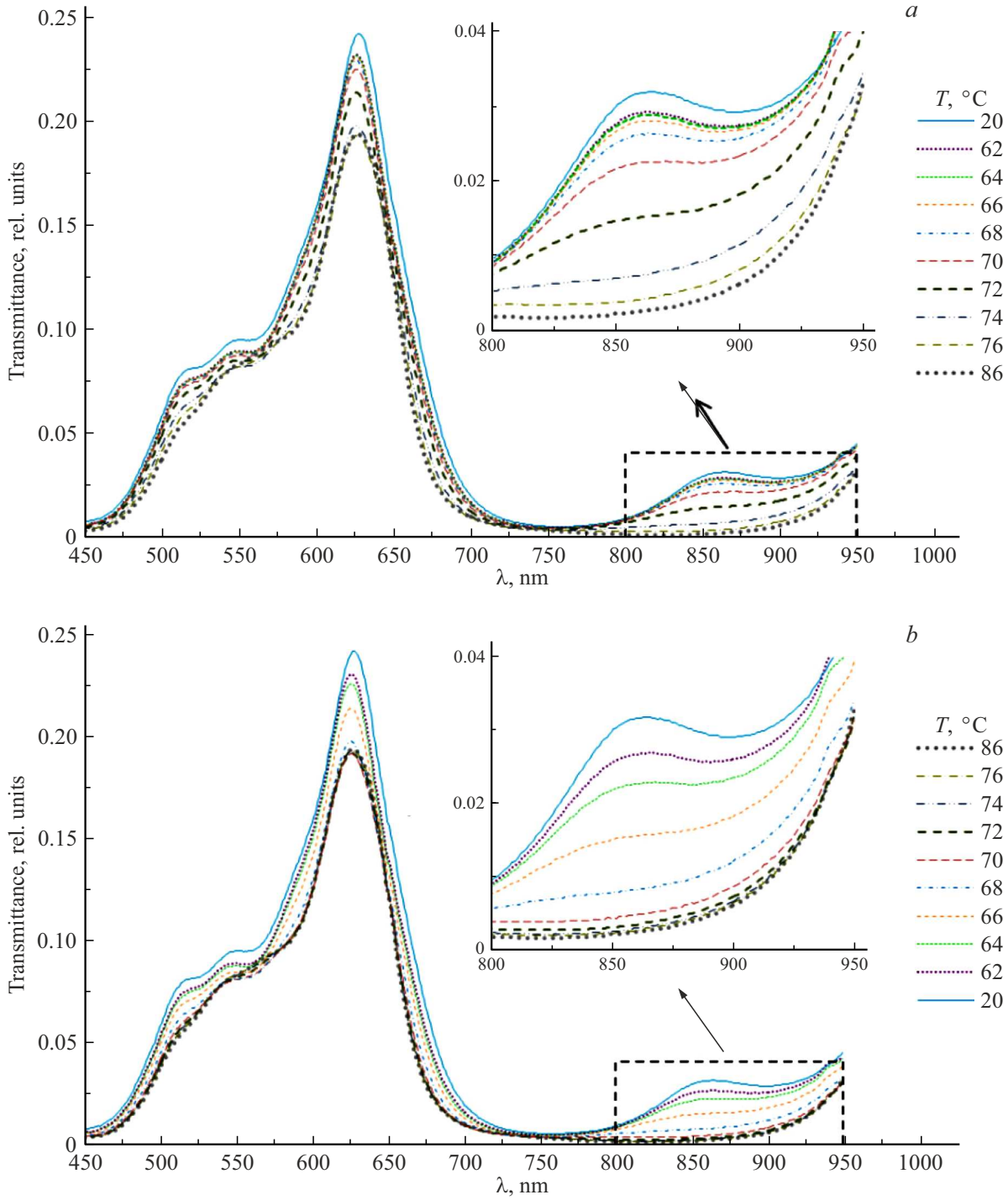

Figure 6. Transmittance spectra of IR-range photon-crystalline structure GGG/$[SiO_2/TiO_2]^4/VO_2/[TiO_2/SiO_2]^4$ (thickness $h_{VO_2} = 163$ nm) during temperature variation: (*a*) heating; (*b*) cooling (the insets show enlarged sections).

Thus, a decrease in the real term of the complex refractive index VO_2 similarly leads to a shift of the transmittance maximum to the region of shorter wavelengths by about 15 nm, and an increase in the imaginary component of the refractive index results in the strong absorption of light in VO_2 half-wave layer up to complete degradation of the resonance peak upon reaching a temperature of 74 °C and more. Thus, at a temperature of 90 °C, the maximum transmittance of the structure for $\lambda = 862$ nm declines by more than 10 times compared to the initial state. As the sample cools (Fig. 6, *b*), a reverse process of Fabry-Perot resonance peak shift and transmittance increasing at the resonance point is observed. It is essential to note that, similarly to a photonic crystal in the visible range at the

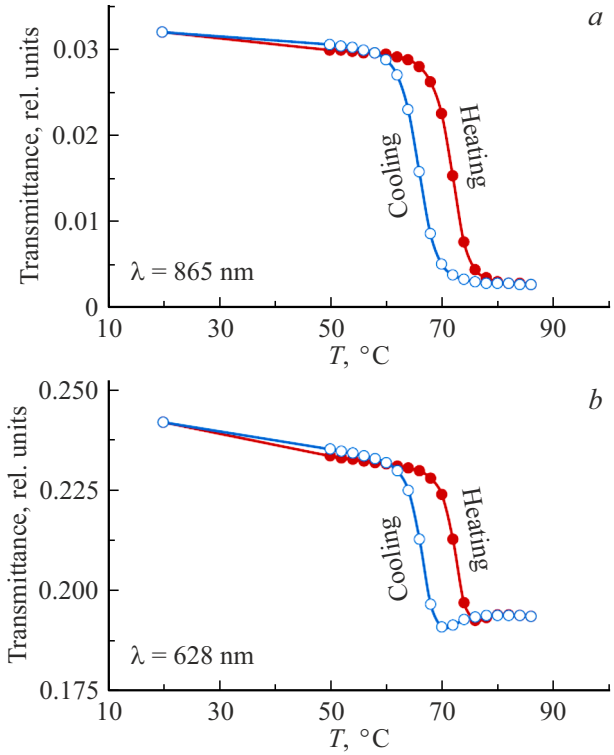

Figure 7. Loops of transmittance temperature hysteresis for the IR range photon-crystalline structure at various wavelengths $\lambda = 865$ nm (a) and $\lambda = 628$ nm (b).

same temperatures, the transmittance spectra upon heating and cooling of the sample exhibit a clear temperature hysteresis with an identical state at the extreme temperature points of 20 and 90 °C.

The analyzed temperature hysteresis of transmittance at various wavelengths during phase transition in VO_2 layer is illustrated in Fig. 7. It can be seen that a change in the optical constants of VO_2 functional layer leads to a significant variation of the structure transmittance by 12 times at the wavelength of $\lambda = 865$ nm in the vicinity of Fabry-Perot resonance (Fig. 7, a) and by 1.25 times at $\lambda = 628$ nm located outside the photon band gap (Fig. 7, b). The width of the transmittance temperature hysteresis loop remains unchanged and makes 6 °C irrespective of the wavelength.

Thus, it can be seen that in IR-range photonic crystal containing an optical half-wave layer VO_2 with a thickness gradient, it is also possible to retune Fabry-Perot optical resonance both parametrically by changing the working area along the thickness gradient of the functional layer VO_2, and thermally by changing its optical constants.

4. Conclusion

Thus, it is possible to create tunable photonic crystal structures for micro- and nanophotonics based on functional half-wave layers VO_2 enclosed between two optical Bragg mirrors. At the same time, varying the thickness of the functional and optical layers makes it possible to create structures with a variable optical spectral range in both, visible and near-infrared bands.

The formation of optical half-wave functional layers with a thickness gradient along the selected direction allows to retune the parameters and control the resonance of the photonic crystals by changing the illumination area at different points of the gradient, which leads to a change in the geometric path difference of rays interfering in the vanadium dioxide layer. A change in the optical characteristics of VO_2 layer as a result of phase transition „semiconductor–metal“ with a change in temperature allows to make thermal tuning and control of the resonant properties of photonic crystals by changing the optical path difference of interfering rays in the functional layer.

These effects of changing the resonant conditions in photonic crystals can also be used in design of various temperature sensors, motion sensors, etc.

Funding

This work was supported by V.I. Vernadsky Crimean Federal University within the project MOL/2024/2.

References

[1] N.V. Morozov, K.P. Galstyan. Tekhnika, Tekhnologii. Inzheneriya, **3** (9), 1 (2018).
[2] S.E. Svyakhovsky, N.I. Pyshko. VMU. Seriya 3. Fizika. Astronomiya, **78** (4), 2340401 (2023) (in Russian). DOI: 10.55959/MSU0579-9392.78.2340401
[3] M.V. Rybin, M.F. Limonov. UFN, **189** (8), 881 (2019). DOI: 10.3367/UFNr.2019.03.038543
[4] D.N. Sovyk, V.G. Ralchenko, D.A. Kurdyukov, S.A. Grudinkin, V.A. Kazakov, S.S. Savin, V.G. Golubev, V.S. Sedov. Estestvennye i matematicheskie nauki 113 (2013)**12**, 113 (2013) (in Russian).
[5] P.D. Garcia, J.F. Galisteo-Lopez, C. Lopez. Appl. Phys. Lett., **87**, 201109 (2005). DOI: 10.1063/1.2132068
[6] V.G. Golubev, V.A. Kosobukin, D.A. Kurdyukov, A.V. Medvedev, A.B. Pevtsov. Semiconductors, **35** (6), 680 (2001).
[7] A.V. Skripal, D.V. Ponomarev, O.M. Ruzanov, I.O. Timofeev. Izvestiya Saratovskogo universiteta. Novaya seriya. Ser. Fizika, **20** (1), 29 (2020). DOI: 10.18500/1817-3020-2020-20-1-29-41
[8] Yu.V. Gulyaev, A.N. Lagarkov, S.A. Nikitov. Vestnik RAN, **78** (5), 438 (2008).
[9] M. Soljacic, J. Joannopoulos. Nature Materials, **3** (4), 211 (2004). DOI: 10.1038/nmat1097
[10] A.S. Abramov, D.A. Korobko, V.A. Lapin, P.P. Mironov. Bull. Lebedev Physics Institute, **51** (1), S1 (2024). DOI: 10.3103/S1068335624600219.
[11] I. Chremmos, O. Schwelb, N. Uzunoglu. *Photonic microresonator research and applications* (Springer Science + Business Media, N.Y., 2010). DOI: 10.1007/978-1-4419-1744-7

[12] J. Heebner, R. Grover, T. Ibrahim. *Optical microresonators: theory, fabrication, and applications* (Springer Science+Business Media, N.Y., 2008). DOI: 10.1007/978-0-387-73068-4
[13] E.A. Kadomina, E.A. Bezus, L.L. Doskolovitch. Komp'yuternaya optika, **2**, 40 (164) (2016) (in Russian). DOI: 10.18287/2412-6179-2016-40-2-164-172
[14] L. Sangwook, H. Kedar; Y. Fan, H. Jiawang, K. Changhyun, S. Joonki, L. Kai, W. Kevin, U.J. Jeffrey. Science, **355** (6323), 371 (2017). DOI: 10.1126/science.aag0410
[15] A.B. Pevtsov, S.A. Grudinkin, A.N. Poddubny, S.F. Kaplan, D.A. Kurdyukov, V.G. Golubev. FTP, **44** (12), 1585 (2010) (in Russian).
[16] F. Scotognella. Front. Photonics, **4**, 1081521 (2023). DOI: 10.3389/fphot.2023.1081521
[17] A. Rashidi, A. Hatef, A. Namdar. Appl. Phys. Lett., **113**, 101103 (2018). DOI: 10.1063/1.5040365
[18] J. Liang, P. Li, X. Song, L. Zhou. Appl. Phys. A, **123** (12), 794 (2017). DOI: 10.1007/s00339-017-1420-5
[19] M. Sun, M. Taha, S. Walia, M. Bhaskaran, S. Sriram, W. Shieh, R.R. Unnithan. Sci. Rep., **8**, 11106 (2018). DOI: 10.1038/s41598-018-29476-6
[20] A.A. Akhmadeev, E.V. Sarandaev, M.Kh. Salakhov. J. Physics: Conference Series, **461** (1), 012022 (2013). DOI: 10.1088/1742-6596/461/1/012022
[21] J. Sun, G.K. Pribil. Appl. Surface Sci., **421**, 819 (2017). DOI: 10.1016/j.apsusc.2016.09.125
[22] C. Lopez. Advanced Materials, **15** (20), 1679 (2003). DOI: 10.1002/adma.200300386
[23] H. Miguez, C. Lopez, F. Meseguer, A. Blanco, L. Vazquez, R. Mayoral, M. Ocana, Y. Fornes, A. Mifsud. Appl. Phys. Lett., **71** (9), 1148 (1997). DOI: 10.1063/1.119849
[24] A. Blanco, E. Chomski, S. Grabtcak, M. Ibisate, S. John, S.W. Leonard, C. Lopez, F. Meseguer, H. Miguez, J.P. Mondia, G.A. Ozin, O. Toader, H.M. Driel. Nature, **405** (25), 437 (2000). DOI: 10.1038/35013024
[25] A.A. Syrov, S.D. Lyashko, A.L. Kudryashov, I.A. Nauhatsky, V.N. Berzhansky, S.V. Tomilin. Physics of Metals and Metallography, **125** (12), 1325 (2024). DOI: 10.31857/S0015323024120049
[26] S.V. Tomilin, V.N. Berzhansky, A.S. Yanovsky, O.A. Tomilina. J. Surf. Investigation: X-ray, Synchrotron and Neutron Techniques, **10** (4), 868 (2016). DOI: 10.1134/S1027451016040376
[27] V.A. Klimov, I.O. Timofeeva, S.D. Khanin, E.B. Shadrin, A.V. Ilyinsky, F. Silva-Andrade. FTP, **37**, 4 (388) (2003) (in Russian).
[28] P.C. Boboc, O.E. Hutanu, A.M. Bragadireanu. Romanian J. Physics, **69**, 906 (2024). DOI: 10.59277/RomJPhys.2024.69.906
[29] A. Ilyinsky, V. Klimov, S. Khanin, E. Shadrin. News of A.I. Herzen State Pedagogical University of Russia,**15**, 100 (2006).
[30] R. Beaini, B. Baloukas, S. Loquai, J.E. Klemberg-Sapieha, L. Martinu. Sol. Energy Mater. Sol. Cells, **205**, 110260 (2020). DOI: 10.1364/OIC.2019.MC.5
[31] M.M. Qazilbash, A.A. Schafgans, K.S. Burch, S.J. Yun, B.G. Chae, B.J. Kim, H.T. Kim, D.N. Basov. Phys. Rev. B, **77**, 115121 (2008). DOI: 10.1103/PhysRevB.77.115121

Translated by T.Zorina